Hydrodynamic properties of carbon nanotubes

J. H. Walther,[1] T. Werder,[1] R. L. Jaffe,[2] and P. Koumoutsakos[1,*]
[1]*Institute of Computational Science, ETH Zürich, Switzerland*
[2]*NASA Ames Research Center, Moffett Field, California 94035, USA*
(Received 8 April 2003; revised manuscript received 26 November 2003; published 4 June 2004)

We study water flowing past an array of single walled carbon nanotubes using nonequilibrium molecular dynamics simulations. For carbon nanotubes mounted with a tube spacing of 16.4×16.4 nm and diameters of 1.25 and 2.50 nm, respectively, we find drag coefficients in reasonable agreement with the macroscopic, Stokes-Oseen solution. The slip length is -0.11 nm for the 1.25 nm carbon nanotube, and 0.49 for the 2.50 nm tube for a flow speed of 50 m/s, respectively, and 0.28 nm for the 2.50 nm tube at 200 m/s. A slanted flow configuration with a stream- and spanwise velocity component of 100 ms^{-1} recovers the two-dimensional results, but exhibits a significant 88 nm slip along the axis of the tube. These results indicate that slip depends on the particular flow configuration.

DOI: 10.1103/PhysRevE.69.062201 PACS number(s): 47.10.+g, 68.08.−p, 47.11.+j, 83.50.Rp

The applicability of carbon nanotubes as sensing [1,2] and manipulating devices in biological systems [3,4] depends critically on their static and dynamic properties in aqueous environments. While the static properties of these hydrophobic structures, e.g., solubility [5] and wettability [6,7], are well understood, their dynamic properties, such as steady and unsteady hydrodynamic forces, are to a large extent unknown. Using continuum Navier-Stokes models to study these properties is questionable, in particular since the no-slip velocity boundary condition, usually assumed in these simulations, is known to fail at hydrophobic surfaces. Slip of $[O(40\ \text{nm})]$ has been observed in experiments of water at hydrophobic surfaces [8–11], but the amount of slip at hydrophilic surfaces remains unclear [12,13]. Thus, Castillo *et al.* [14] measured the Brownian motion of C_{60} molecules and found both the slip and no-slip condition to hold depending on the type of solvent. The slip is characterized by a finite velocity (ΔU) at the fluid-solid interface, with the slip length (L_s) defined as the proportionality coefficient between ΔU and the local fluid shear rate (du/dy), where u denotes the velocity component tangential to the wall and y is the normal distance [15].

To study the validity of the no-slip boundary condition and to determine the hydrodynamic forces acting on carbon nanotubes, we conduct nonequilibrium molecular dynamics (NEMD) simulations for water flowing past an array of single walled carbon nanotubes. Previous molecular dynamics simulations of slip have mostly considered simple geometries such as Poiseuille [16,17] and the planar Couette flows [18,19]. Most of these studies have considered Lennard-Jones fluids confined between Lennard-Jones walls and have demonstrated the presence of slip, no-slip, and locking (negative slip length) depending on the ''corrugation'' of the surface. Thus, no-slip and locking are observed for low density solids while slip is found to occur at strongly nonwetting interfaces and for high density solids. Richardson [20] found that the no-slip condition is a consequence of the surface roughness, and similar conclusions were obtained in MD simulations of alkanes in a Couette flow between two sinusoidal walls [21]. However, the situation is less clear for nanoscale systems where the feature size is comparable to the size of the solvent molecules. For these systems, we expect the amount of slip to be a function of the particular geometry.

In the present NEMD simulations, we use the SPC/E water model [22] with fixed bond lengths and angles, constrained using the SHAKE algorithm [23]. The carbon nanotube is modeled as a rigid structure to facilitate the analysis of the slip velocity at the water carbon nanotube interface [7]. The treatment of the solid wall as a rigid structure was recently found to play a minor role in the significant amount of slip observed for methane at graphite and carbon nanotube surfaces, cf. Sokhan *et al.* [24,25]. The carbon-water interaction is described by a Lennard-Jones potential acting between the carbon atoms and the water oxygens. As parameters we use a carbon-oxygen van der Waals radius (σ_{CO}) of 3.19 Å [26] and a well depth ϵ_{CO} of 0.4389 kJ mol^{-1} [27]. This potential reproduces the experimental contact angle of water on graphite of 86° [27]. The interactions are truncated at 1 nm using a smooth tapering of the potential [28].

The mean onset flow velocity is adjusted by scaling the velocity of the center of mass of the water molecules in a 3 nm long inlet region (L_i) upstream of the carbon nanotube, cf. Fig. 1. The results were found to be insensitive to the particular value of L_i with a 7% increase in the slip length when using $L_i=1.5$ nm (not shown). Using a leapfrog time discretization scheme, the center of mass velocity ($\boldsymbol{v}_{com}$) of the water molecules in the inlet region is updated according to

$$\boldsymbol{v}_{com}^{n+1/2}=\boldsymbol{v}_{com}^{n-1/2}+(\delta t/m_{tot}^{n})(\boldsymbol{f}_{tot}^{n}+\boldsymbol{b}_{tot}^{n}), \tag{1}$$

where $\boldsymbol{f}_{tot}$ is the total force acting on the center of mass of the molecules in the inlet region, $\boldsymbol{b}_{tot}$ is the total body force, and δt is the time step. In Eq. (1), $\boldsymbol{b}_{tot}$ is adjusted to yield the desired center of mass velocity ($\boldsymbol{v}_{com}^{n+1/2}=\boldsymbol{U}$), thus

$$\boldsymbol{b}_{tot}^{n}=(m_{tot}^{n}/\delta t)(\boldsymbol{U}-\boldsymbol{v}_{com}^{n-1/2})-\boldsymbol{f}_{tot}^{n}. \tag{2}$$

This forcing is imposed throughout the simulation and results in a boundary condition equivalent to prescribing the total mass flow through the system and allows a nonuniform inlet velocity profile. Combining the forcing with periodic

*Electronic address: petros@inf.ethz.ch

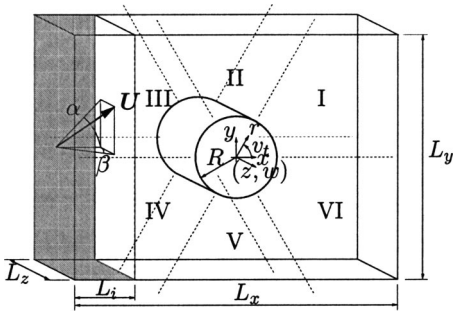

FIG. 1. Sketch of the carbon nanotube-water system. R denotes the radius of the carbon nanotube, L_x and L_z the size of the system in the stream and spanwise directions, and L_y is the height of the computational box. The center of mass velocity of the water molecules contained in the shaded ''inlet'' region (L_i) is fixed to obtain the desired onset flow velocity ($\boldsymbol{U}$). The angle of attack is determined by the angles α and β. The Secs. I–VI refer to the polar sampling regions.

boundary conditions, we effectively model the flow past an array of carbon nanotubes arranged in an in-line (L_x,L_y) configuration.

The simulations involve water flowing past arrays of (16,0) or (32,0) zigzag carbon nanotubes with diameters of 1.25 and 2.50 nm, respectively. The carbon nanotube is located at the center of the computational box of dimension $16.4\times16.4\times2.1$ nm^3. The total number of water molecules is approximately 18 500, and the carbon nanotubes consist of 320 and 640 atoms for the 1.25 and 2.50 nm tubes, respectively. The onset flow speed (U) is set at 50, 100, and 200 ms^{-1} corresponding to low Mach numbers, but sufficiently above the thermal noise to allow efficient sampling. This ensures an incompressible flow and avoids appreciable viscous heating during the simulation. The hydrodynamic speed of sound in SPC/E water at physiological conditions is $a\approx1450$ ms^{-1} [29] resulting in Mach numbers (Ma $=Ua^{-1}$) for the present simulations less than 0.15. To study the influence of the flow periodicity, we furthermore conduct a simulation with an onset flow speed of 100 ms^{-1} and an angle of attack (α) of 17°. Finally, we consider a slanted onset flow with velocity components of 100 ms^{-1} along the x and z axes, corresponding to an angle of attack (β) of 45°.

During the first 4 ps of the 40 ps equilibration, the volume of the computational box is adjusted to match the target density of water, $\rho=0.997$ g cm^{-3} in the far field, i.e., in the region defined by $r>R+\delta$. R is the radius of the carbon nanotube and $\delta=0.8$ nm is chosen to exclude the region containing the density variations of the water in the vicinity of the carbon nanotube [28]. The adjustment of the volume is performed by scaling the computational box in the x-y plane (see Fig. 1), while keeping the extent of the box in the z-direction fixed. The carbon nanotube is excluded from the scaling to preserve the radius of the tube. The flow is initially quiescent and impulsively turned on after 6 ps. During the first 8 ps of the equilibration, the temperature of the system is controlled using a Berendsen thermostat, and the remaining 32 ps of the equilibration is required to establish a steady flow. During the 380 ps simulations the system temperature increases due to viscous heating, which for the 50, 100, and 200 ms^{-1} cases, amount to 0, 9, and 40 K, respectively. The thermostat is nevertheless turned off during the sampling to avoid any bias introduced by the heat bath [30]. The results are sampled after the 40 ps equilibration at intervals of 0.2 ps for a total of 1700 samples. The hydrodynamic forces for the 50 and 100 ms^{-1} cases reach stable mean values after 30–40 ps, whereas the viscous heating in the 200 ms^{-1} simulation results in a reduction of the fluid viscosity, and a subsequent reduction of the drag force ($\approx-35\%$ in 340 ps). The cases studied are listed in Table I.

TABLE I. Molecular dynamics simulation results. D denotes the diameter of the carbon nanotube, U is the onset flow speed, Re denotes the Reynolds number, L_s is the slip length, C_d^{Oseen} represents the Stokes-Oseen drag coefficient, and C_d^{MD} is the drag coefficient extracted from the MD simulations. The Re numbers and drag coefficients shown in parenthesis are the estimated values at elevated temperatures caused by the viscous heating.

Case	D (nm)	U (ms^{-1})	Re		L_s (nm)	C_d^{Oseen}		C_d^{MD}
1	1.25	50	0.0685		−0.11	104		138±18
2	2.50	50	0.137		0.49	76		88±11
3	2.50	100	0.274	(0.337)	0.27	46	(40)	40±3
4	2.50	200	0.548	(1.11)	0.28	29	(20)	15±2
5	2.50	100[a]	0.274	(0.337)	0.33	46	(40)	36±3
6	2.50	100[b]	0.274		0.40/88	46		37±4

[a]The onset flow speed for case 5 is 100 ms^{-1} with an angle of attack of $\alpha=17°$.

[b]For case 6, the onset flow speed is 100 ms^{-1} in the x-y plane and 100 ms^{-1} along z axis (W), thus $\beta=45°$. Two slip lengths are extracted for this case in the x-y and r-z planes, respectively.

We present the results in terms of the time averaged profile of the density and streaming velocity

$$\rho_k=\frac{1}{V_k}\sum_i^{n_k} m_i, \quad \boldsymbol{v}_k=\sum_i^{n_k} m_i\boldsymbol{v}_i \Big/ \sum_i^{n_k} m_i, \tag{3}$$

where m_i and $\boldsymbol{v}_i$ are the mass and velocity of the ith water molecule, and n_k denotes the number of molecules in the kth bin of volume V_k. Statistics are sampled in polar bins with a resolution of 200 and 1600 radial bins (with a radial spacing of 0.040 and 0.005 nm) for the velocity and density profiles, respectively. The circumferential direction has 6 bins corresponding to the six sections shown in Fig. 1. We find that both the density and velocity profiles exhibit symmetry across the x axis, whereas asymmetries are discernible in the density profiles in the streamwise direction near the carbon nanotube, cf. Fig. 2. The locations of the density maxima are similar for the three radial profiles, with the first peak located at $r-R=0.32$ nm coinciding with the carbon-oxygen van der Waals radius (σ_{CO}). However, the peak values decrease from 3.1 g cm^{-3} for the upstream direction (Sec. III) to 2.8 g cm^{-3} and 2.5 g cm^{-3} for Secs. II and I, respectively. Since the far-field density is constant with a value of approximately 1.00 g cm^{-3}, the observed asymmetry is ascribed to the local compression of the water near the front stagnation point.

The amount of slip experienced for these systems is extracted from the tangential component (v_t) of the streaming

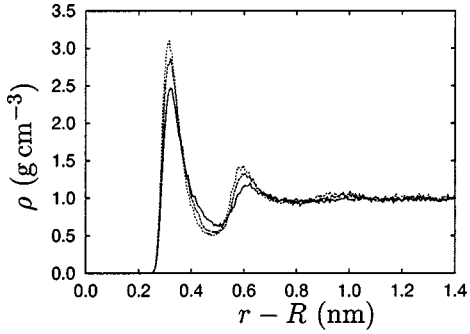

FIG. 2. The time averaged radial density profile of water flowing past an array of carbon nanotubes. The diameter of the carbon nanotube is 2.50 nm and the onset flow speed 100 ms^{-1} (case 3). The profiles are sampled upstream (- -, Sec. III), at the midsection (– –, Sec. II), and downstream section (—, Sec. I).

velocity [Eq. (3)] for Secs. II and V which is shown in Fig. 3. The velocity profiles for the different cases are similar, but reach different free-stream values due to the different blockage $[(D-L_y)/L_y]$ experienced by the flow. Since the Reynolds number ($\mathrm{Re}=\rho UD/\mu$), based on the tube diameter and the fluid viscosity ($\mu=0.91$ cP [31]), is less than unity (cf. Table I), the velocity profiles are fitted to the Stokes velocity field for a single circular cylinder [32]

$$v_t = a\ln(r/R) + b + c(R^2/r^2), \tag{4}$$

where a, b, and c, are parameters of the fit. From this we obtain the slip velocity as $\Delta U = b+c$, and the slip length as

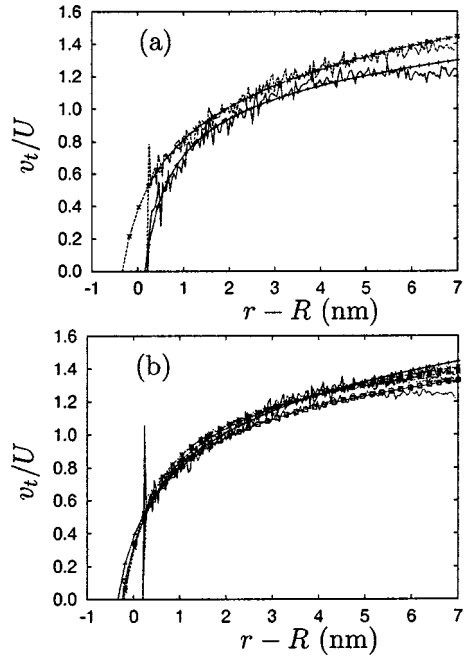

FIG. 3. The time averaged tangential component of the streaming velocity for the flow past an array of carbon nanotubes. The measured profiles are sampled from Secs. II and V and compared with a fit to Eq. (4). The velocity profiles for the different diameter tubes are presented in (a) 1.25 nm: —, measured; –+–, fit; 2.50 nm, – –, measured; –×–, fit. The velocity profiles for the 2.50 nm at different flow speeds is shown in (b) 50 ms^{-1}: —, measured; –+–, fit; 100 ms^{-1}: – –, measured; –×–, fit; 200 ms^{-1}: - -, measured; -*-, fit; 100 ms^{-1} at 17°: ···, measured; -□-, fit.

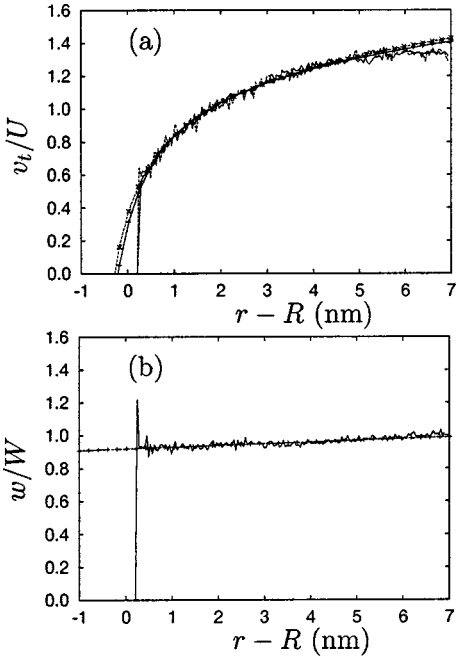

FIG. 4. The time averaged tangential (a) and axial (b) component of the streaming velocity for the three-dimensional flow past an array of carbon nanotubes (case 6). The measured tangential profile (–×– and - -) is sampled from Secs. II and V and compared with a fit to Eq. (4), and to the corresponding results (–+– and —) from the two-dimensional flow (case 3) . The axial profiles were found to be similar for all the six sections, and a combined average is fitted to the linear profile $w(r)=a+br$.

$L_s = R(b+c)(a-2c)^{-1}$. The fit is performed for the data shown in Fig. 3 in the interval $r \in [R+\sigma_{CO}:7\ \mathrm{nm}]$.

The velocity profiles from the simulations of carbon nanotubes with diameters of 1.25 and 2.50 nm and a flow speed of 50 ms^{-1} are similar and show good agreement with the Stokes velocity profile cf. Fig. 3(a). The estimated slip lengths for the 1.25 and 2.50 nm tubes are -0.11 and 0.49 nm, respectively. Thus, while previous studies of nonpolar liquids have demonstrated a significant slip at dense surfaces [25,24], and preliminary studies of water in a planar Couette flow [33] have indicated a persistent slip in the range 30–60 nm for system pressures of 1–1000 bar, the present flow configuration of water passing a small, high-curvature, hydrophobic object indicates a significantly reduced slip length. This result is confirmed when we consider the flow past the 2.50 nm carbon nanotubes at flow speeds of 50, 100, and 200 ms^{-1} and at 100 m/s for 17° incidence; cf. Fig. 3(b). For all four cases the velocity profiles are very similar with slip lengths of 0.49, 0.27, 0.28, and 0.33 nm, respectively. Another simulation (not shown) was conducted for a flow speed of 400 ms^{-1} (Ma$\approx$0.3), which despite strong viscous heating, also experiences a slip length of $O(\sigma_{CO})$. Thus, while the slip velocity remains non-negligible for the 2.5 nm tube ($\Delta U/U \approx 0.3$, cf. Fig. 3), the stagnation points of the flow retard the molecules in that region sufficiently to prevent any significant slip at the boundary. The molecules hitting the stagnation point do not have sufficient time to overcome their deceleration as they are transported around the carbon nanotube. The influence of the flow periodicity seems

negligible when comparing the two simulation at 100 ms^{-1} at zero and 17° angle of attack. Thus, the no-slip condition emerges as a result of the flow past a particular geometry which, to the flow, appears as a ''corrugated'' surface. This conjecture is supported by the amount of slip extracted from the slanted flow study (case 6). The slip length in the *x*-*y* plane [Fig. 4(a)] is 0.40 nm and consistent with the two-dimensional simulations, whereas a significant slip length of 88 nm is observed in the *r*-*z* plane [Fig. 4(b)].

Finally, we consider the fluid forces ($\boldsymbol{F}$) acting on the carbon nanotube array by computing the total time-averaged force on the carbon atoms. The streamwise component of the force (F_x) is compared with the approximate Stokes-Oseen drag for the flow past an array of two-dimensional circular cylinders [34]

$$C_d^{Oseen} = C_d^{cc} \frac{3 + 2\phi^{5/3}}{3 - \frac{9}{2}\phi^{1/3} + \frac{9}{2}\phi^{5/3} - 3\phi^2}, \tag{5}$$

where ϕ is the fraction of the volume occupied by the carbon nanotube [here $\phi = \pi R^2 (L_x L_y)^{-1}$], and C_d^{cc} is the drag coefficient on a single circular cylinder given by [32]

$$C_d^{cc} = 8\pi/\mathrm{Re}\ln(7.4/\mathrm{Re}). \tag{6}$$

The measured drag coefficients [$C_d^{MD} = F_x(\frac{1}{2}\rho U^2 L_z D)^{-1}$] are sampled in 17 blocks of 20 ps each, and the resulting mean values and standard deviations are shown in Table I. The comparison between C_d^{MD} and the approximate Stokes-Oseen solution for an array of circular cylinders reveals a reasonable agreement. The deviations for the 50 ms^{-1} simulations amount to 31% and 16% for the 1.25 and 2.50 nm carbon nanotubes, respectively. The simulations of the 2.50 nm carbon nanotube at onset flow speeds of 50, at 100, and 200 ms^{-1}, and at 100 m/s for 17° angle of attack, and the slanted flow configuration show deviations of 16%, −13%, −48%, −21%, and −20%, respectively. However, the viscous heating of 8 and 40 K experienced in the 100 and 200 ms^{-1} cases results in reduced fluid viscosities ($\mu_{308^\circ} \approx 0.74$ cP and $\mu_{340^\circ} \approx 0.45$ cP) leading to drag coefficients of 40 and 20, respectively. This brings the measured drag coefficients to within 25% of the Stokes-Oseen solution. The two-dimensional flow cases (1–5) allow us to use a thermostat in the homogeneous (*z*) direction. The simulation at 200 ms^{-1} (case 4) was repeated with the thermostat (not shown) to verify the consistency of the predicted slip and drag forces. The measured slip length was $O(\sigma_{CO})$ (0.42 nm), and the drag coefficient remained constant throughout the simulation with a mean value of 19 ± 1, corresponding to a −34% deviation. Increasing the effective diameter of the cylinder to account for the water-tube stand off distance does not appreciably alter this agreement.

In conclusion, we have presented NEMD simulations of water flowing past an array of carbon nanotubes with diameters of 1.25 and 2.50 nm. For flow speeds in the interval 50–200 ms^{-1} we find that the slip length in the plane of the carbon nanotube is comparable to the van der Waals distance of the carbon-water potential. We conjecture that the no-slip condition is related to the presence of the stagnation point of the flow, and hence to the particular geometry. Simulation of a slanted flow configuration confirms this, as we recover the no-slip condition in the plane of the carbon nanotube and a significant slip along the axis of the tube. The hydrodynamic forces acting on the carbon nanotube are furthermore found to be in good agreement with the macroscopic Stokes-Oseen solution for the flow past an array of circular cylinders.

[1] K. Moloni *et al.*, Ultramicroscopy **80**, 237 (1999).
[2] J. Li *et al.*, Surf. Interface Anal. **28**, 8 (1999).
[3] F. Balavoine *et al.*, Angew. Chem. **38**, 1912 (1999).
[4] C.V. Nguyen *et al.*, Nano Lett. **2**, 1079 (2002).
[5] E. Dujardin *et al.*, Advanced Mat. **10**, 1472 (1998).
[6] E. Dujardin *et al.*, Science **265**, 1850 (1994).
[7] T. Werder *et al.*, Nano Lett. **1**, 697 (2001).
[8] H. Helmholtz and G. von Piotrowski, Sitzungsber. Kaiserlichen Akad. Wiss. **40**, 607 (1860).
[9] E. Schnell, J. Appl. Phys. **27**, 1149 (1956).
[10] N.V. Churaev, V.D. Sobolev, and A.N. Somov, J. Colloid Interface Sci. **97**, 574 (1984).
[11] J. Baudry *et al.*, Langmuir **17**, 5232 (2001).
[12] O.I. Vinogradova and G.E. Yakubov, Langmuir **19**, 1227 (2003).
[13] E. Bonaccurso *et al.*, Phys. Rev. Lett. **88**, 076103 (2002).
[14] R. Castillo, C. Garza, and S. Ramos, J. Phys. Chem. **98**, 4188 (1994).
[15] J.C. Maxwell, Philos. Trans. R. Soc. London **170**, 231 (1879).
[16] J.-L. Barrat and L. Bocquet, Phys. Rev. Lett. **82**, 4671 (1999).
[17] K.P. Travis and K.E. Gubbins, J. Chem. Phys. **112**, 1984 (2000).
[18] P.A. Thompson and S.M. Troian, Nature **389**, 360 (1997).
[19] M. Cieplak *et al.*, Phys. Rev. Lett. **86**, 803 (2001).
[20] S. Richardson, J. Fluid Mech. **59**, 707 (1973).
[21] A. Jabbarzadeh *et al.*, Phys. Rev. E **61**, 690 (2000).
[22] H.J.C. Berendsen *et al.*, J. Phys. Chem. **91**, 6269 (1987).
[23] W.F. van Gunsteren and H.J.C. Berendsen, Mol. Phys. **37**, 1311 (1977).
[24] V.P. Sokhan *et al.*, J. Chem. Phys. **117**, 8531 (2002).
[25] V.P. Sokhan *et al.*, J. Chem. Phys. **115**, 3878 (2001).
[26] M.J. Bojan and W.A. Steele, Langmuir **3**, 1123 (1987).
[27] T. Werder *et al.*, J. Phys. Chem. B **107**, 1345 (2003).
[28] J.H. Walther *et al.*, J. Phys. Chem. B **105**, 9980 (2001).
[29] U. Balucani *et al.*, Phys. Rev. E **47**, 1677 (1993).
[30] K.P. Travis *et al.*, J. Chem. Phys. **103**, 10638 (1995).
[31] P.E. Smith and W.F. van Gunsteren, Chem. Phys. Lett. **215**, 315 (1993).
[32] G. K. Batchelor, *An Introduction To Fluid Dynamics*, 1st ed. (Cambridge University Press, Cambridge, 1967).
[33] J. H. Walther, R. Jaffe, T. Werder, T. Halicioglu, and P. Koumoutsakos, in *Proceedings of the Summer Program 2002*, edited by Parviz Moin, Nagi N. Mansour, and Peter Bradshaw (Center for Turbulence Research, Stanford University/NASA Ames, 2002), pp. 317–329.
[34] R. F. Probstein, *Physicochemical Hydrodynamics* (Butterworths, London, 1989).